Mapping the Energy Surface for the Folding Reaction of the Coiled-Coil Peptide GCN4-p1†

Beatriz Ibarra-Molero,‡ George I. Makhatadze,§ and C. Robert Matthews*,‡

Department of Chemistry, Life Sciences Consortium, and Center for Biomolecular Structure and Function, The Pennsylvania State University, University Park, Pennsylvania 16802, and Department of Biochemistry and Molecular Biology, Pennsylvania State College of Medicine, Hershey, Pennsylvania 17033-0850

Received June 23, 2000; Revised Manuscript Received November 16, 2000

ABSTRACT: The energy surface for the folding/unfolding reactions of the homodimeric coiled-coil peptide M2V GCN4-p1, a 33-residue segment comprising the leucine zipper domain of the transcriptional activator GCN4, was mapped by equilibrium and kinetic methods. Circular dichroism (CD) spectroscopy was used to monitor the urea-induced unfolding reaction at a series of temperatures and temperature-induced unfolding at a series of urea concentrations. A global analysis of the urea- and temperature-induced equilibrium unfolding data provides strong support for a two-state mechanism. The absence of a detectable population of intermediate states is also consistent with differential scanning calorimetry and thermal CD melts as a function of peptide concentration. Furthermore, a global analysis of stopped-flow CD kinetic data is consistent with a kinetic two-state mechanism as well. The urea dependence of the apparent folding and unfolding rate constants at a series of temperatures reveals that the activation enthalpy and entropy for unfolding in the absence of denaturant are both significantly greater than those for the refolding reaction. Although the unfolding barrier is dominated by the activation enthalpy, the activation entropy dominates the refolding barrier. The relative magnitudes of the urea dependence of the unfolding and refolding rate constants indicate that 55−65% of the surface area is buried in the transition state. The activation parameters imply a partially organized transition state and are consistent with a previous model in which the pair of C-terminal heptad repeats are docked in a coiled-coil-like motif [Zitzewitz et al. (2000) *J. Mol. Biol. 296*, 1105−1116].

The existence of multisubunit proteins in all forms of life is thought to reflect their increased stability and the opportunities for cooperativity in ligand binding, allosteric control of enzyme activity, and rate enhancement in sequential metabolic reactions (*1*). Therefore, understanding the mechanism by which the formation of secondary, tertiary, and quaternary structures is coordinated in the folding of multimeric proteins and the specific nature of subunit−subunit interactions have become pivotal issues in the protein folding field.

A quantitative assessment of the folding and assembly of multisubunit proteins requires equilibrium studies of the stable states and kinetic studies of transition states and any transient intermediates. Energy surfaces for the folding and unfolding reactions have been mapped for many monomeric proteins (see, for example, refs *2*−*9*). However, the inherently more complex folding mechanisms usually observed for multimeric proteins have limited the information available for these systems. Thermodynamic characterization of transition states and/or intermediates has been reported for only a few such proteins, e.g., *Escherichia coli* Trp repressor (*10*, *11*), P22 arc repressor (*12*), ROP (*13*, *14*), and hGST A1-1 (*15*). The structural complexity of these dimeric systems has limited the insights obtained.

One of the simplest model systems for studying protein−protein interactions is the two-stranded, parallel coiled-coil motif. First postulated by Crick (*16*), the structure is comprised of two right-handed α helices that wrap around each other to form a left-handed superhelix. The amino acid sequence is characterized by a heptad repeat, $(abcdefg)_n$, in which hydrophobic residues in the a and d positions and oppositely charged residues in the e and g positions form the dimer interface. One of the better studied members of a large class of coiled-coil peptides is GCN4-p1, the 33-residue leucine zipper domain of the yeast transcriptional activator GCN4. This small fragment adopts a stable, well-folded dimeric form that has enabled high-resolution structural analysis by both NMR (*17*, *18*) and X-ray crystallography (*19*).

Some of the thermodynamic parameters characterizing the folding/unfolding transition of GCN4-p1 and several analogues have been reported. A simple two-state monomer−dimer equilibrium for the thermally induced unfolding reaction and the urea-induced unfolding reaction is supported by differential scanning calorimetry (DSC)[1] and circular dichroism (CD) spectroscopy, respectively (*20*−*25*). However, recent NMR results by Holtzer and co-workers (*26*−

† This work was supported by the National Institutes of Health Grants GM54836 to C.R.M. and GM54537 to G.I.M. Partial support for B.I.-M. was provided by an FPI Postdoctoral Fellowship from the Spanish Ministry of Education and Culture.

* To whom correspondence should be addressed. E-mail: crm@psu.edu. Phone: (814) 865-8859. Fax: (814) 863-8403.

‡ The Pennsylvania State University.

§ Pennsylvania State College of Medicine.

10.1021/bi001438e CCC: $20.00
Published on Web 12/29/2000

28) suggest that a more complex model is required to explain the site-specific data. A simple two-state kinetic mechanism has been postulated for GCN4-p1 and various GCN4-based analogues, on the basis of both CD and fluorescence measurements (*22*, *25*, *29*, *30*). Two-state mechanisms have also been reported for other designed homodimeric (*24*, *31*) and heterodimeric (*32*) coiled-coil systems. By contrast, multistep folding has been reported for the GCN4 leucine zipper (*33*) and for related analogues (*34*) when the folding reaction is probed using extrinsic fluorescent labels attached to the amino terminus. The discrepancies between these studies may result from the introduction of the spectroscopic probe or from the different experimental approaches.

The potential simplicity of the thermodynamic and kinetic behavior of the GCN4-p1 peptide allows for a quantitative analysis of the energy surface of the folding reaction for this model coiled-coil system. A previous mutational analysis of GCN4-p1 (*35*) led to the proposal that the dimeric transition-state ensemble is principally comprised of preformed helical C-terminal heptads that dock in a coiled-coil-like fashion. This interpretation is in marked contrast with an early study by Sosnick and co-workers (*30*), who concluded that the formation of helical structure in the transition state must occur after the bimolecular collision event.

A systematic study of the temperature- and urea-induced unfolding and refolding reactions of M2V GCN4-p1, in which the readily oxidized Met at position 2 is replaced by Val, provided quantitative assessments of the relative thermodynamic properties of the dimeric native state, the dimeric transition state, and the monomeric unfolded state. Hydrogen bond formation and the exclusion of solvent from nonpolar surfaces appear to play significant roles in defining the energy surface for the folding reaction.

MATERIALS AND METHODS

Peptide Purification. A variant of GCN4-p1 (*19*) in which Met at position 2 is replaced by Val, was employed to avoid undesirable oxidation products. The peptide was also acetylated at the amino terminus and amidated at the carboxy terminus to eliminate electrostatic contributions from the formal charges at the termini. The peptide M2V GCN4-p1, Ac−RVKQLEDKVEELLSKNYHLENEVARLKKLVGER−NH_2, was purchased from Biomolecules Midwest Inc. (St. Louis, MO). The purity of the peptide was greater than 95%, as was determined by the presence of a single peak by analytical reverse-phase HPLC. Electrospray mass spectroscopy characterization of this purified peptide yielded a molecular mass of 4005.6 Da (MW_{calc} = 4006.7 Da).

Reagents and Experimental Conditions. Ultrapure guanidine HCl and urea were purchased from ICN Biomedicals Inc. (Costa Mesa, CA). Urea was further purified by passage of aqueous solutions of about 9.5 M through an AG 501-X8 (D) ion-exchange resin (Bio-Rad, Hercules, CA) prior to adding the buffer components. All other chemicals were reagent grade. Spectra/por 2000 MWCO dialysis membrane was purchased from Spectrum (Houston, TX). Deionized and degassed water was used throughout. The buffer conditions used in all the experiments were 50 mM sodium phosphate, pH 7.0, and 150 mM sodium chloride. Peptide concentrations were determined spectrophotometrically in 6 M GdnHCl by monitoring the absorbance of the only chromophore (Tyr 17) at 276 nm using an extinction coefficient of 1500 M^{-1} cm^{-1} (*36*). Guanidine and urea concentrations were determined from refraction index measurements (*37*).

DSC. Calorimetric experiments were performed as described previously (*38*), using a VP-DSC microcalorimeter (Microcal, Northampton, MA; *39*) with cell volumes of 0.52 mL, under an excess pressure of 30 psi to prevent boiling at high temperatures. The scan rate was 1 °C min^{-1} in all cases. Aqueous stock solutions of the peptide were prepared by exhaustive dialysis at 4 °C against the buffer solution. The peptide concentrations in terms of monomer ranged from 105 to 422 μM. Aggregation was observed when the calorimetric experiment was performed at higher peptide concentrations. The reversibility after two cycles of heating and cooling was determined to be greater than 90% in all cases.

Equilibrium CD Studies. The experiments were carried out using an AVIV 62DS CD spectrometer equipped with a thermoelectric temperature controller. A Hamilton 500 Microlab automatic titrator was attached to the CD and controlled via an external computer. Far-UV CD spectra from 270 to 220 nm were taken using a bandwidth of 2.5 nm, a signal-averaging time of 2 s, and a 1.0 nm step size.

Two sets of thermal unfolding experiments were collected in order to study peptide and urea concentration effects. In the absence of urea, the peptide concentration ranged from 10 to 200 μM, and cell path lengths of 1−5 mm were used. When studying the urea effect on thermal denaturation (experiments were done at 0, 0.54, 1.0, and 3.0 M urea), peptide concentrations were between 12 and 23 μM and the cell path length was 5 mm. In all cases, the spectra were collected from 5 to 85 °C. Equilibration times of 3−7 min were used depending on the temperature. All transitions are highly reversible (greater than 95%), as is shown by the recovery of the CD signal at 222 nm after cooling the peptide solution from 85 to 4 °C. The degree of reversibility decreases to ~80% when the exposure time at high temperature is increased, especially in the presence of urea. Under these conditions, irreversible processes such as aggregation or chemical modification of the peptide are more likely to occur.

The equilibrium urea-induced denaturation of M2V GCN4-p1 was studied by CD measurements at 2.5 °C increments within the temperature range of 5−40 °C. Stock solutions of native peptide in buffer and unfolded peptide in 9.5 M urea were mixed in the desired amounts to vary the final denaturant concentration in 0.2 M increments from 0 to 8.5 M using the automatic titrators. Prior to the measurements,

[1] Abbreviations: ΔASA_{apol}, change in apolar accessible surface area; ΔASA_{pol}, change in polar accessible surface area; $[\theta]_{222}$, mean residue ellipticity measured at 222 nm; CD, circular dichroism; C_p, partial molar heat capacity; DSC, differential scanning calorimetry; GCN4-p1, coiled-coil region derived from the yeast transcriptional activator GCN4 (residues 249−281); GdnHCl, guanidine hydrochloride; ΔH_{cal}, calorimetric enthalpy; ΔH_{vH}, van't Hoff enthalpy; k_a, preexponential factor; k_{corr}, apparent rate constant corrected for urea viscosity; k_{obs}, observed rate constant; M2V GCN4-p1, variant of GCN4-p1 in which the naturally occurring methionine in position 2 is replaced with a valine; N_2, native dimer; T_m, melting temperature (temperature at which the fraction of the native state is 0.5); $T°$, temperature at which $\Delta G = 0$; ‡, transition state; U, unfolded state; X_i, molar fraction of the state i; $\Delta Y°$, variation of the thermodynamic property Y at 1 M standard-state dimer concentration; η, viscosity in the presence of denaturant; η_0, viscosity in the absence of denaturant.

the peptide was allowed to equilibrate for a time sufficient to ensure that the denaturation equilibrium was reached (5−10 min, depending on the temperature and the urea concentration). Control experiments were carried out by preparing the samples manually and waiting 1 h prior to collecting the data. Similar results were obtained with both procedures, ensuring that the samples were fully equilibrated during the automated titration experiments. The final peptide concentration ranged from 10 to 30 μM. Reversibility was found to be greater than 95% for the urea-induced unfolding within the temperature range studied by titrating the peptide solution in high urea (∼9.5 M) with a solution of peptide in buffer.

Analytical Ultracentrifugation. Equilibrium ultracentrifugation data were collected on a Beckman XL-I analytical centrifuge. Absorbance as a function of radial distance was monitored at 237, 277, and 285 nm for peptide concentrations of 10, 50, 100, 200, 300, and 400 μM using an eight-cell rotor rated at 50 000 rpm. Equilibrium sedimentation experiments were run at 40 000 rpm for >36 h until equilibration was reached. The temperature for all the experiments was 15 °C. Data were analyzed as described previously (*40*).

Unfolding and Refolding Kinetic Experiments. The change in the ellipticity signal at 222 nm with time was monitored using an AVIV 202SF stopped-flow CD spectrometer. The temperature was controlled by Peltier elements in the mixer/optical cell assembly and syringe drive. Temperature probes in these locations measured the actual temperature, and two software controlled feedback loops allocated power to the Peltier elements. Kinetic measurements were carried out at 10, 15, 20, 25, 27.5, 30, and 35 °C, yielding a total of 303 experimental traces. For the unfolding experiments, the peptide was initially in buffer. For the refolding kinetics, the peptide was allowed to equilibrate in high concentrations of urea (5.5−7.5 M) for 1 h at the desired temperature prior to initiation of the refolding reaction. The reaction was initiated in each case after a rapid 10- or 7-fold dilution of the appropriate peptide solution into the buffer containing different concentrations of urea. Because the refolding reaction is peptide concentration dependent, at least two different sets of data at different peptide concentrations were collected to ensure the reliability of the results. Typical final peptide concentrations ranged from 10 to 28 μM. The cell path length was 1 mm, the bandwidth was 2.5 nm, and the dead time was 5 ms (*41*). An average of 19 shots were collected per trace to enhance the signal-to-noise ratio.

DATA ANALYSIS

Equilibrium. All the equilibrium unfolding profiles were analyzed according to a two-state dimeric model in which only the native dimer (N_2) and unfolded monomer (U) are significantly populated:

$$N_2 \leftrightarrows 2U \tag{1}$$

The relative amounts of each species at a given temperature are determined from the denaturation equilibrium constant, K, at that temperature:

$$K = \frac{[U]^2}{[N_2]} = \frac{2P_T X_U^{\,2}}{1 - X_U} \tag{2}$$

where P_T stands for the total peptide concentration in terms of monomer ($P_T = 2[N_2] + [U]$). The fraction of unfolded form, X_U, can be easily obtained from eq 2:

$$X_U = \frac{\sqrt{K(T)^2 + 8P_T K(T)} - K(T)}{4P_T} \tag{3}$$

In this paper, all the thermodynamic properties are expressed per mole of dimer.

DSC Data Analysis. The thermograms were corrected for the instrumental (solvent−solvent) baseline, scan rate, and peptide concentration in each case, using the software provided by Microcal (Northampton, MA). The partial heat capacity of the peptide in solution was determined by using a value of 0.753 mL g^{-1} for the partial specific volume, calculated from the amino acid sequence (*42*). The temperature dependence of the partial molar heat capacity function is described by the following expression (*43*−*45*):

$$C_p(T) = C_p^{N_2}(T)\,[1 - X_U(T)] + C_p^{U}(T)\,X_U(T) + C_p^{exc}(T) \tag{4}$$

where $C_p^{N_2}$ and C_p^{U} are the partial molar heat capacities of the native and unfolded states, given by the pre- and post-transition baselines in the experimental profiles, respectively. The excess heat capacity, C_p^{exc}, corresponds to the heat absorbed during the unfolding reaction and can be written as

$$C_p^{exc}(T) = \frac{\Delta H^\circ_{vH}}{RT^2}\,\frac{\Delta H^\circ_{cal} X_U (1 - X_U)}{2 - X_U} \tag{5}$$

where ΔH°_{cal} is the calorimetric enthalpy and ΔH°_{vH} is the van't Hoff enthalpy which gives the temperature dependence of the denaturation equilibrium constant, K. It was assumed that the temperature dependence of the enthalpies may be neglected within the comparatively narrow range of the calorimetric transition. The calorimetric enthalpy was assigned at T_m, the temperature at which $X_{N_2} = 0.5$ (*45*). In the data analysis, a linear dependence of the partial heat capacities of the native and unfolded states with temperature was considered:

$$C_p^{N_2}(T) = C_{p,ref}^{N_2} + \alpha T \tag{6}$$

$$C_p^{U}(T) = C_{p,ref}^{U} + \beta T \tag{7}$$

Because the native and unfolded baselines were experimentally very well defined in all cases, the actual values for the y intercepts and slopes ($C_{p,ref}^{N_2}$, $C_{p,ref}^{U}$, α, and β) were not allowed to vary during the fitting process. The heat capacity change was considered temperature-independent because it has been shown to be a good approximation within the temperature range from 0 to 80 °C (*46*, *47*). The heat capacity change between N_2 and U, ΔC_p, was then obtained, extrapolating the pre- and post-transition baselines to T_m. The temperature dependence of the free-energy change is given by the Gibbs−Helmholtz equation:

$$\Delta G^\circ(T) = -RT \ln K(T) = \Delta H^\circ_{vH}(T_m)\,(1 - T/T_m) + \Delta C_p[T - T_m - T \ln(T/T_m)] - RT \ln K(T_m) \tag{8}$$

where $K(T_m)$ is equal to P_T (see eq 2).

The experimental profiles were fit using eq 4 [expanded through eqs 2−8], where T_m, ΔH°_{cal} and ΔH°_{vH} were the adjustable parameters.

CD Data Analysis. (1) Thermal Unfolding in the Absence of Urea. The thermal denaturation profiles at 222 nm and at different peptide concentrations were analyzed assuming a two-state model as described by eq 1. The observed mean residue ellipticity is given by

$$[\theta] = [\theta_{N_2}](1 - X_U) + [\theta_U]X_U \quad (9)$$

where $[\theta_{N_2}]$ and $[\theta_U]$ are the mean residue ellipticities corresponding to the folded dimer and unfolded monomer, respectively. On the basis of the experimental data, $[\theta_{N_2}]$ was assumed to vary linearly with temperature:

$$[\theta_{N_2}] = [\theta_{N_0}] + \gamma T \quad (10)$$

where $[\theta_{N_0}]$ and γ are the *y* intercept and slope, respectively; by contrast, $[\theta_U]$ was considered to be independent of temperature. Equation 9 together with eqs 2, 3, 8, and 10 was used to perform nonlinear, least-squares fitting to the experimental profiles. The temperature dependence of the denaturation enthalpy was neglected within the narrow temperature range over which the transition takes place. Nevertheless, no significant change in the resulting fitting parameters was observed when ΔC_p was fixed to the calorimetric value.

(2) Global Analysis of Urea Titration Experiments and Thermal Denaturation Experiments in the Presence of Urea. Individual fits to the urea titrations and thermal melts in the presence of urea were carried out initially. The linear extrapolation method was assumed to estimate the peptide stability in the absence of urea (*48*, *49*):

$$\Delta G^\circ = \Delta G^\circ_{H_2O} - m[\text{urea}] \quad (11)$$

where *m* is the dependence of free energy on the denaturant concentration. Linear dependencies of the native and unfolded baselines with respect to the urea concentration and temperature were assumed, based upon the experimental profiles. Equations 2, 3, 8, 9, and 11 were used in the fitting process. To obtain more accurate thermodynamic parameters and also to help in model discrimination, isothermal urea titrations between 5 and 40 °C together with thermal denaturation data in the presence of urea were simultaneously fitted to a simple two-state dimeric model. A matrix of 26 experimental profiles describing the change in the CD signal at 222 nm along three axes (urea concentration, temperature, and peptide concentration) was globally analyzed using the in-house software package Savuka 5.2. It was assumed that ΔC_p does not change either with temperature or urea concentration and that the *m* value is temperature-dependent. The fitting parameters globally linked throughout the data set were T_m, ΔS°_m, ΔC_p, the *y* intercept and slope values defining the temperature dependence of *m*, and the spectroscopic properties corresponding to the native state. The total protein concentration and the parameters describing the unfolded baselines were considered as local parameters in the fitting routine. The resulting values obtained for the peptide concentration were within 10% of the expected values.

Kinetic Data Analysis. Local fits of the data to a single-exponential rate equation for unfolding and a second-order bimolecular association reaction for refolding were performed (*50*). However, local fits to individual kinetic traces do not provide a reliable estimate of the rate constants in the transition region because both the refolding and the unfolding reactions contribute significantly to the observed rate constant. To obtain accurate values for the rate constants in water and also to improve the reliability of the results, a global analysis of the traces is required. Thus, the unfolding and refolding traces collected at the same temperature over an extended urea concentration range (0.6−8 M) were globally fit to a two-state kinetic mechanism (*50*) as described previously (*22*). A linear dependence of the activation free energies on the urea concentration was assumed (5*1*). Transition-state theory relates the microscopic rate constant with the denaturant concentration as follows (*52*):

$$k_i = k_{i,H_2O} \exp(m_{i\rightarrow\ddagger}[\text{urea}]/RT) \quad (12)$$

When the fitting was performed, the following parameters were globally linked through the experimental traces: the rate constants for refolding ($k_{U\rightarrow\ddagger}$) and unfolding ($k_{N_2\rightarrow\ddagger}$) at 0 M urea and the parameters $m_{U\rightarrow\ddagger}$ and $m_{N_2\rightarrow\ddagger}$, which describe the urea effect on the rate constants for refolding and unfolding, respectively. The molar ellipticities of the native dimer, $[\theta_{N_2}]$, and the unfolded monomer, $[\theta_U]$, at a particular urea concentration were calculated from the corresponding baselines in the equilibrium urea titration profile at the same temperature. These values were fixed during the fitting routine and were used to determine the initial fraction of unfolded monomer in each case. The peptide concentration was allowed to vary to account for small offsets in the instrument and/or uncertainty in the concentration measurement. In all cases, the resulting peptide concentrations were within 10% of the measured concentrations.

The resulting urea dependence of the unfolding and refolding rate constants at each temperature was corrected for the effect of urea on viscosity according to (*53*)

$$\ln k_{corr} = \ln k_i + \ln(\eta/\eta_0) \quad (13)$$

where k_{corr} is the apparent rate constant after the viscosity correction and η and η_0 are the viscosities in the presence and in the absence of the denaturant at 25 °C. Data for η/η_0 as a function of urea concentration was taken from ref *54*. It was assumed that the temperature dependence of η/η_0 of urea solutions is not significant between 10 and 35 °C (*54*, *55*). The effect of the urea viscosity correction on the extrapolated unfolding rate constants at 0 M urea was found to be within experimental error.

RESULTS

By examination of the equilibrium and kinetic folding properties of M2V GCN4-p1 at a variety of temperatures, urea concentrations, and peptide concentrations, rigorous tests of the mechanism can be applied and quantitative assessments of the thermodynamic parameters can be obtained.

Analytical ultracentrifugation experiments as well as CD spectroscopy were used to confirm that the replacement of Met at position 2 with Val did not perturb the native folded state of GCN4-p1. The dimeric form of the coiled-coil M2V

Table 1: Thermodynamic Parameters Obtained from the Analysis of the DSC Experiments Using the Two-State Denaturation Model $N_2 \leftrightarrows 2U$

P_T[a] (μM)	T_m[b] (K)	ΔH°_{cal} [kcal (mol of dimer)$^{-1}$]	ΔH°_{vH} [kcal (mol dimer)$^{-1}$]	$\Delta H^\circ_{cal}/\Delta H^\circ_{vH}$	ΔC_p[c] [cal (mol of dimer)$^{-1}$ K^{-1}]
422	337.1	52.1	51.6	1.01	372
409	336.9	52.3	50.7	1.03	369
372	336.6	55.1	50.5	1.09	446
334	336.4	46.1	54.0	0.85	264
279	335.4	53.9	50.6	1.06	314
227	334.3	43.6	55.8	0.78	493
200	333.8	49.3	53.8	0.92	471
190	333.6	56.8	51.4	1.10	550
162	333.4	48.7	55.9	0.87	335
105	331.4	53.7	54.6	0.98	451
average[d]		51.2 $\pm$ 4.1	52.9 $\pm$ 2.2	0.97 $\pm$ 0.11	406 $\pm$ 89

[a] Total peptide concentration in terms of monomer. [b] Temperature at which the fraction of native peptide is equal to 0.5. [c] Values obtained by extrapolating the native and unfolded baseline to T_m and measuring the difference between them. [d] Thermodynamic parameters obtained from the average of 10 experiments. Errors correspond to the standard deviation.

GCN4-p1 at 15 °C and within the concentration range from 10 to 400 μM was demonstrated by analytical ultracentrifugation (data not shown). Also, similar secondary structures were observed when comparing the far-UV CD spectra corresponding to the M2V mutant and the wild-type GCN4-p1 peptide. Both spectra were superimposable (data not shown), showing the typical features of an α-helix: two minima at 222 and 208 nm with a ratio of 1.1, consistent with full helical content (*56*). Therefore, the replacement of Met 2 by Val does not perturb the state of association or the secondary structure of this coiled-coil peptide.

Thermal Denaturation. An extensive thermodynamic characterization of the leucine zipper peptide, M2V GCN4-p1, has been carried out based on urea- and heat-induced denaturation experiments. The combination of these two approaches increases the experimentally accessible temperature range, providing a more accurate measurement of the properties governing the conformational transition (*57*, *58*).

The temperature dependence of the partial molar heat capacity corresponding to solutions of different peptide concentrations (105−422 μM) in buffer was obtained by DSC; the results are shown in Figure 1. Plots of C_p versus temperature yield a single asymmetric peak, whose maximum is shifted toward higher temperature as the peptide concentration increases (*43*, *44*, *59*). Fits of each of the scans to a two-state dimeric model yielded excellent agreement (Figure 1), and the calorimetric enthalpies determined from the fits were equivalent to those obtained by integration of the peak area when a smooth third-order spline function was used to connect the pre- and post-transition baselines. The results obtained from the analysis are summarized in Table 1. An average ratio for $\Delta H^\circ_{cal}/\Delta H^\circ_{vH}$ of 0.97 $\pm$ 0.11 was obtained over the concentration range explored, supporting the validity of the two-state assumption (*60*). The average value of ΔC_p was 406 $\pm$ 89 cal (mol of dimer)$^{-1}$ K^{-1}.

The thermal unfolding of M2V GCN4-p1 at peptide concentrations ranging from 10 to 200 μM was also monitored by CD. The sigmoidal transitions observed at 222 nm (Figure 2A) indicate a cooperative disruption of the helical structure with increasing temperature. The midpoint of the transition is concentration-dependent, as is predicted for an unfolding process that is coupled with dissociation. The mean residue ellipticity at 222 nm of M2V GCN4-p1 under native conditions (low temperature) is $\sim -35\,000$ deg cm^2 dmol^{-1}, which is in agreement with the value reported by O'Shea et al. (*61*) for GCN4-p1 and consistent with a full helical structure. The experimental profiles are well-described by the formalism given in eq 1, in which the folded dimers and unfolded monomers are the only states significantly populated. As shown in Figure 2A, there is an excellent agreement between the observed and the predicted denaturation curves.

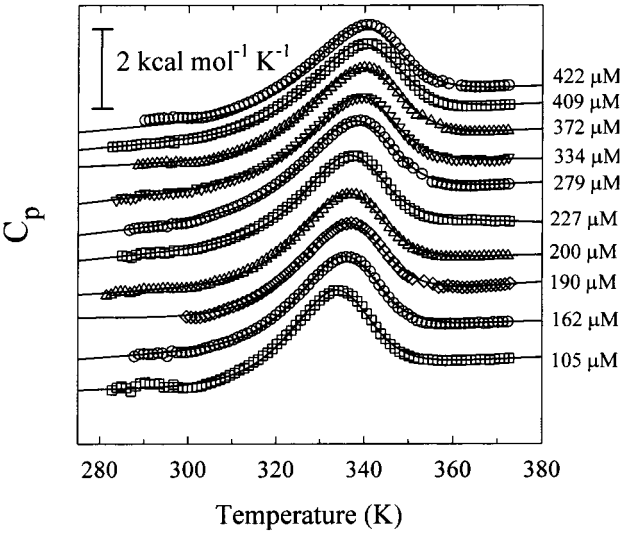

FIGURE 1: DSC profiles for M2V GCN4-p1 unfolding. The protein concentration for each experiment, expressed in terms of monomer, is indicated to the right of the corresponding profile. Buffer conditions were 50 mM sodium phosphate, pH 7.0, and 150 mM NaCl. The solid lines represent the fit of the data to the two-state dimeric model. Curves have been shifted along the *y* axis for display purposes.

Figure 2B displays the dependence of the transition midpoint temperature on the peptide concentration for both the CD and DSC experiments. The small but consistent differences between the two sets of data might reflect heat diffusion processes in the CD cell holder where the thermal isolation is not as effective as that in the calorimetric cells. Values for the van't Hoff unfolding enthalpy and entropy corresponding to the middle of the transition temperature range covered (61.1 °C for DSC and 56.2 °C for CD) were obtained using the following expression (*62*):

$$\frac{1}{T_m} = -\frac{R}{\Delta H^\circ} \ln P_T + \frac{\Delta S^\circ}{\Delta H^\circ} \qquad (14)$$

Table 2: Comparison of the Thermodynamic Parameters at pH 7.0 and 25 °C for the Unfolding of M2V GCN4-p1 Obtained by Different Experimental Approaches[a]

	DSC[b]	CD[b]	kinetic[c] (Eyring)	kinetic[c] (Kramers)
$\Delta H°$ [kcal (mol of dimer)$^{-1}$]	38.6 ± 0.7	36.5 ± 0.1	32.4 ± 4.8	32.4 ± 4.8
$\Delta S°$ [cal (mol of dimer)$^{-1}$ K^{-1}]	96.0 ± 5.8	89.2 ± 3.2	76.0 ± 16.1	80.6 ± 13.5
$\Delta G°$ [kcal (mol of dimer)$^{-1}$]	9.9 ± 2.4	9.9 ± 1.0	9.7 ± 6.7	8.3 ± 6.4

[a] Errors correspond to 2 standard deviations. [b] Parameters extrapolated at 25 °C from those obtained from the dependence of $1/T$ with ln P_T (Figure 2B), as indicated by eq 14. The peptide concentration range was 105−422 μM for DSC and 10−200 μM for CD experiments. [c] Thermodynamic parameters calculated from kinetic values using Eyring and Kramers formalisms (reported in Table 4), according to the equation $\Delta Y°_{kn} = \Delta Y°_{N_2 \rightarrow ‡} - \Delta Y°_{U \rightarrow ‡}$.

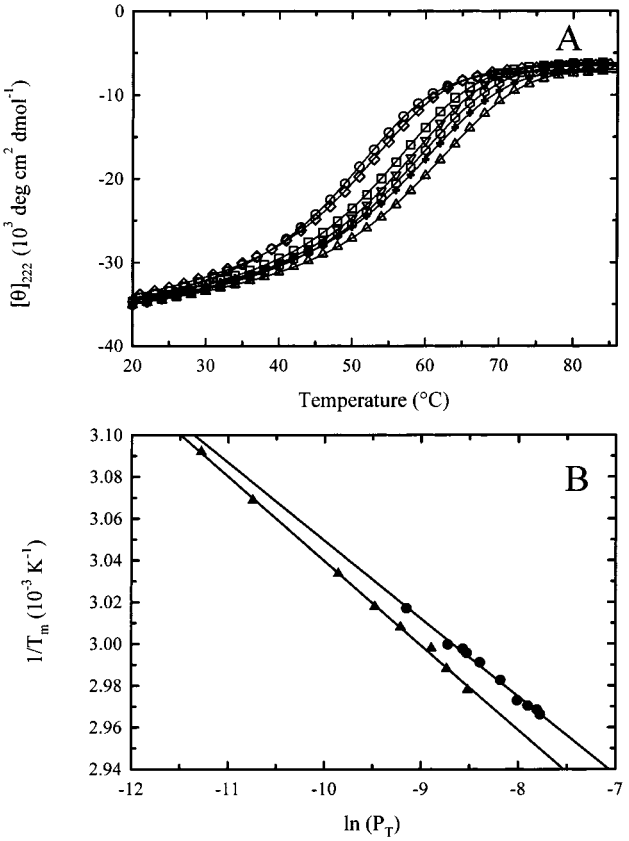

FIGURE 2: (A) Thermal denaturation of M2V GCN4-p1 monitored by CD at 222 nm and at peptide concentrations of 12 (circles), 20 (diamonds), 50 (squares), 76 (inverted triangles), 100 (hexagons), 137 (crosses), and 200 μM (triangles). Profiles are normalized to mean residue ellipticity for comparison. Buffer conditions are described in the caption to Figure 1. The lines represent the fits of the individual data sets to a two-state dimeric equilibrium unfolding model. (B) Plot of the inverse of T_m (defined as the temperature at which $X_{N_2} = 0.5$) versus the natural logarithm of peptide concentration (expressed in terms of monomer). The symbols correspond to CD thermal melts (triangles) and DSC experiments (circles) in the absence of urea, and the solid lines represent the fit of each data set to a straight line.

The values for $\Delta H°$ and $\Delta S°$ at 25 °C were obtained by extrapolation according to eqs 15 and 16 and are summarized in Table 2:

$$\Delta H°(T) = \Delta H°(T_m) + \Delta C_p(T - T_m) \qquad (15)$$

$$\Delta S°(T) = \frac{\Delta H°(T_m)}{T_m} + \Delta C_p \ln(T/T_m) \qquad (16)$$

The thermodynamic parameters obtained using two different techniques, DSC and CD, are in good agreement. Average values for the enthalpy, entropy, and free energy change of unfolding of the dimer under standard conditions are 37.5 kcal (mol of dimer)$^{-1}$, 92.6 cal (mol of dimer)$^{-1}$ K^{-1}, and 9.9 kcal (mol of dimer)$^{-1}$, respectively.

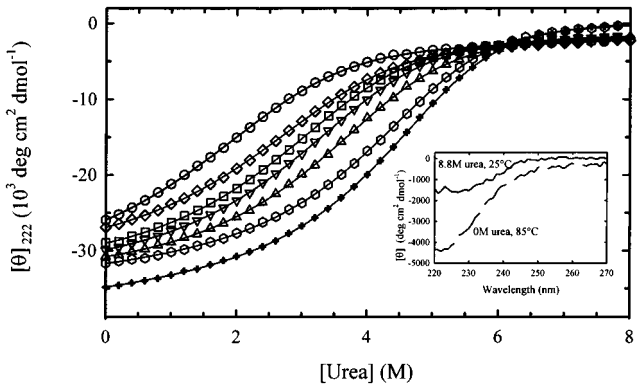

FIGURE 3: Representative urea titrations carried out at 7.5 (crosses), 10 (hexagons), 20 (triangles), 25 (inverted triangles), 27.5 (squares), 32.5 (diamonds), and 40 °C (circles). Profiles are normalized to mean residue ellipticity for comparison. The peptide concentration ranged from 10 to 30 μM. The lines represent the result of a global analysis to a two-state equilibrium model of experimental profiles corresponding to urea titrations (20 traces) and thermal melts in the presence of urea (6 traces). The inset shows the CD spectra of the urea-induced (solid line) and temperature-induced (dashed line) unfolded states of M2V GCN4-p1, respectively, at the given conditions.

Urea Denaturation. CD was also used to monitor the urea-induced denaturation of M2V GCN4-p1. A total of 20 urea-induced denaturation curves was collected at temperatures ranging from 5 to 40 °C. A representative subset of these data is shown in Figure 3. As expected, an increase in temperature correlates with a decrease in the resistance of the peptide to chemical denaturation. A slight increase in the ellipticity of the unfolded baseline was observed in the temperature range from 5 to 15 °C, possibly resulting from enhanced urea binding at low temperature. The thermally induced unfolding of M2V GCN4-p1 in the presence of various urea concentrations (from 0 to 3 M) was also studied. Increasing denaturant concentration leads to a monotonic decrease in the transition midpoint temperature (data not shown).

The solid lines in Figure 3 represent the global analysis of the entire set of data represented by the 26 urea- or temperature-induced (in the presence of urea) unfolding curves. The thermodynamic parameters obtained at 1 M standard state peptide concentration are $\Delta C_p = 556 \pm 10$ cal (mol of dimer)$^{-1}$ K^{-1}, $\Delta S° = 188 \pm 1$ cal (mol of dimer)$^{-1}$ K^{-1}, $T° = 95.8 \pm 0.1$ °C, $m_{25°C} = 0.82 \pm 0.06$

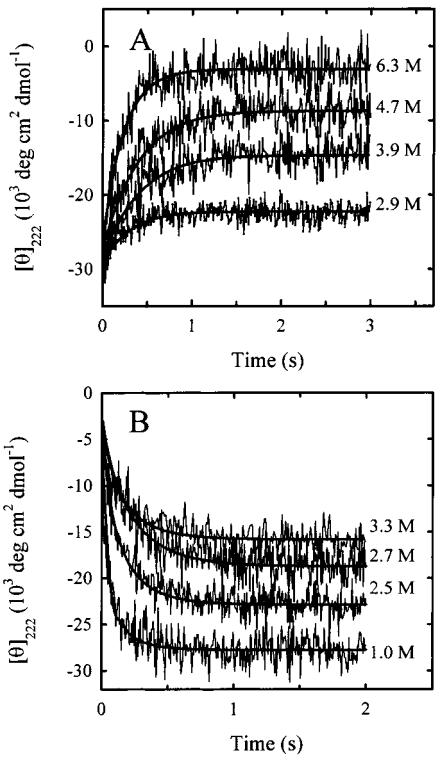

FIGURE 4: Representative kinetic traces for unfolding and refolding of the M2V GCN4-p1 peptide at 20 °C, normalized to mean residue ellipticity for comparison. (A) Unfolding from 0 M urea to the final urea concentration indicated alongside each trace. (B) Refolding from ~6 M urea to the final urea concentration indicated alongside each trace. Lines represent the results of a global analysis of 26−56 combined refolding and unfolding traces for each temperature studied. Buffer conditions are described in the caption to Figure 1.

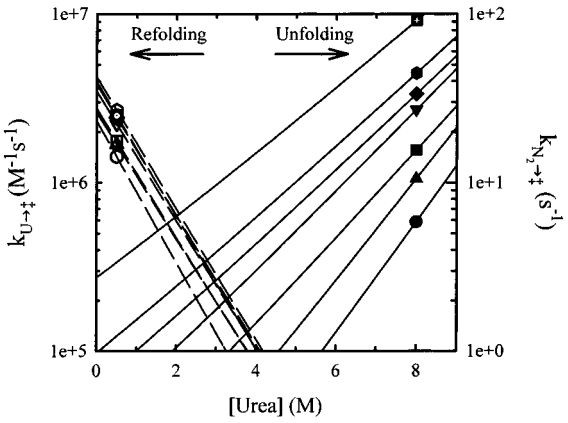

FIGURE 5: Urea dependence of the refolding (dashed lines) and unfolding (solid lines) rate constants for M2V GCN4-p1 at 10 (circle), 15 (triangle), 20 (square), 25 (inverted triangle), 27.5 (diamond), 30 (hexagon), and 35 °C (cross); note that symbols do not represent experimental data. Lines represent the result of performing a global fit of 26−56 unfolding and refolding kinetic traces for each temperature studied. Correction for the urea viscosity effect was made according to eq 13. Buffer conditions are described in the caption to Figure 1.

kcal M^{-1} (mol of dimer)$^{-1}$, and $dm/dT = (-7.1 \pm 0.3) \times 10^{-3}$ kcal M^{-1} (mol of dimer)$^{-1}$ K^{-1}.

A comparison between the far-UV CD spectra corresponding to the thermally induced and urea-induced unfolded states is displayed in the inset in Figure 3. The significant difference between these two spectra suggests that the thermally induced unfolded monomer has a higher residual helical content.

Kinetic Studies. The change in ellipticity at 222 nm with time was monitored after rapid dilution of the peptide solution into solutions with different final urea concentrations. Representative subsets of unfolding and refolding traces at 20 °C are displayed in Figure 4, parts A and B, respectively. For all temperatures studied, unfolding data is well-described by a single-exponential rate equation, whereas a second-order bimolecular association reaction is required to describe the refolding data. Although the inherently low signal-to-noise ratio of CD spectroscopy could mask a more complex response, similar experiments using fluorescence detection to monitor the folding of Y17W GCN4-p1 do not reveal any additional kinetic phases (*63*). In all cases, the good agreement between the mean residue ellipticity signal at infinite time and the equilibrium signal at comparable denaturant concentrations indicates that no slow reactions take place (data not shown). Furthermore, because less than 10% of the far-UV CD signal (the limit of detection) develops in the dead time of the instrument, 5 ms, for both unfolding and refolding reactions, rapidly formed intermediates, if present, are not measurably populated. This result is consistent with the observed exponential dependence of the rate constants obtained from the fits of individual kinetic traces on the denaturant concentration (data not shown; *51*). Deviations from this simple behavior at low and/or high urea concentrations, termed "roll-over" in the chevron plots (*64*), would imply the presence of intermediates.

A global analysis to a two-state kinetic model ($N_2 \leftrightarrows 2U$) was performed over all kinetic traces collected at the same temperature. The resulting urea dependence of the unfolding and refolding rate constants, i.e., the chevron plot (*51*), for each temperature after correction for urea viscosity is depicted in Figure 5. The rate constants for refolding ($k_{U\rightarrow\ddagger}$) and unfolding ($k_{N_2\rightarrow\ddagger}$) in the absence of denaturant and the $m_{U\rightarrow\ddagger}$ and $m_{N_2\rightarrow\ddagger}$ parameters, describing the urea effect on the activation Gibbs energies for refolding and unfolding, respectively, are listed in Table 3. The predominant effect of temperature on the rate constants is observed for the unfolding reaction: $k_{N_2\rightarrow\ddagger}$ increases by 170-fold from 10 to 35 °C, whereas $k_{U\rightarrow\ddagger}$ only increases by ~2-fold. Although $m_{U\rightarrow\ddagger}$ displays no significant dependence on temperature, $m_{N_2\rightarrow\ddagger}$ diminishes as the temperature increases.

The equilibrium parameters can be calculated from the kinetic results by using the standard relations $\Delta G°_{kn} = -RT \ln(k_{N_2\rightarrow\ddagger}/k_{U\rightarrow\ddagger})$ and $m_{kn} = m_{N_2\rightarrow\ddagger} - m_{U\rightarrow\ddagger}$. As is shown in Table 3, there is an excellent correspondence between the $\Delta G°$ and m values obtained from equilibrium and kinetic experiments. The same monotonic decrease of these parameters with increasing temperature is observed in both approaches.

Arrhenius Analysis. The temperature dependence of the unfolding and refolding rate constants in the absence of denaturant was analyzed according to the Arrhenius equation:

$$\ln k_i = \ln A_i - E_{a,i}/RT \qquad (17)$$

where E_a represents the activation energy and A_i is the preexponential term. The Arrhenius plots for refolding and unfolding, shown in Figure 6, parts A and B, respectively, are well-described by linear fits. It has previously been shown

Table 3: Parameters from the Global Fits of the Unfolding and Refolding Kinetic Data Analyzed According to the Eyring Formalism and Comparisons with the Equilibrium Results

T^a	$k_{U\rightarrow\ddagger} \times 10^{-6\,b}$	$k_{N_2\rightarrow\ddagger} \times 10^{\,b}$	$m_{U\rightarrow\ddagger}{}^c$	$m_{N_2\rightarrow\ddagger}{}^c$	$\Delta G°_{kn}{}^d$	$m_{kn}{}^d$	$\Delta G°{}^e$	m^e
10.0	2.32	0.16	−0.53	0.42	10.58	0.95	10.49	0.98
15.0	2.60	0.48	−0.48	0.39	10.21	0.87	10.27	0.96
20.0	2.75	1.53	−0.50	0.33	9.74	0.83	9.86	0.91
25.0	3.48	3.74	−0.51	0.32	9.52	0.83	9.54	0.89
27.5	3.81	6.24	−0.52	0.30	9.34	0.82	9.36	0.88
30.0	4.23	9.73	−0.53	0.29	9.22	0.82	9.19	0.85
35.0	3.97	27.40	−0.55	0.27	8.69	0.82	8.77	0.87

[a] Temperature expressed in °C. [b] Refolding and unfolding rates in the absence of urea, $k_{U\rightarrow\ddagger}$ in units of M^{-1} s^{-1} and $k_{N_2\rightarrow\ddagger}$ in units of s^{-1}, respectively, were determined from the global fits of the data to the two-state model. Errors are ±10%. [c] $m_{U\rightarrow\ddagger}$ and $m_{N_2\rightarrow\ddagger}$ represent the urea dependence of the refolding and unfolding rate constants, respectively, in units of kcal (mol of dimer)$^{-1}$ M^{-1} obtained from the global fits of the data and after correction for the urea viscosity effect according to eq 13. Errors are ±0.05 kcal (mol of dimer)$^{-1}$ M^{-1}. [d] Free-energy change of unfolding of the dimer in the absence of urea and *m* value in units of kcal (mol of dimer)$^{-1}$ and kcal (mol of dimer)$^{-1}$ M^{-1}, respectively, were calculated from the global analysis of the kinetic data. [e] Free-energy change of unfolding of the dimer in the absence of urea and *m* value in units of kcal (mol of dimer)$^{-1}$ and kcal (mol of dimer)$^{-1}$ M^{-1}, respectively, were obtained from the individual fits of the corresponding urea titration. Errors are ±0.2 kcal (mol of dimer)$^{-1}$ and ±0.05 kcal (mol of dimer)$^{-1}$ M^{-1} for $\Delta G°$ and *m*, respectively.

that curvature is observed in the Arrhenius plot if the reaction occurs with a significant change in the activation heat capacity (*2*, *4*, *65*−*67*). The absence of significant curvature within the temperature range explored in this work made it impossible to determine the change in heat capacity values for the refolding or unfolding reactions. The values for the refolding and unfolding activation energies can be extracted from the slope of the linear fits shown in Figure 6, parts A and B: $\Delta E°_{aU\rightarrow\ddagger} = 2.8 \pm 0.9$ kcal (mol of dimer)$^{-1}$ and $\Delta E°_{aN_2\rightarrow\ddagger} = 35.2 \pm 3.9$ kcal (mol of dimer)$^{-1}$.

The activation entropy, $\Delta S°_{i\rightarrow\ddagger}$, can be estimated from the observed rate constant, k_{obs}, and the activation enthalpy using transition-state theory:

$$k_{obs} = k_a \exp\left(\frac{-\Delta G°_{i\rightarrow\ddagger}}{RT}\right) = k_a \exp\left(\frac{-\Delta H°_{i\rightarrow\ddagger}}{RT}\right) \exp\left(\frac{\Delta S°_{i\rightarrow\ddagger}}{R}\right) \quad (18)$$

where the exponential term(s) represents the activation free-energy barrier that must be surmounted for the reaction to proceed. The validity of using transition-state theory for analyzing the data is supported by the fact that single-exponential unfolded kinetics were always observed under the different experimental conditions explored (10−35 °C and 0.6−8.0 M urea). Also, simple second-order bimolecular reactions were observed for the refolding process. These experimental facts suggest a single activation barrier for unfolding and refolding. The magnitude of the preexponential factor, k_a, depends on the formalism chosen. The Eyring formalism was developed initially for describing simple chemical reactions in the gas phase and represents an upper limit for estimating the value of k_a. According to the Eyring formalism (*68*), $k_a = k_B T/h = 6.2 \times 10^{12}$ s^{-1} at 25 °C, where *h* and k_B are the Planck and Boltzmann constants, respectively. Despite widespread use of Eyring's theory to model protein folding rates (*2*−*4*, *7*, *69*), there are some limitations when it is applied to complex conformational changes in macromolecules. Those limitations include the role of the solvent, entropic considerations related to the ensemble nature of the states involved in the reaction, and the existence of a complex reaction coordinate. By contrast, Kramers' model (*70*) provides a more realistic approach to study reactions in the condensed phase and protein folding because it explicitly considers the contribution of Brownian motion in the formation of the encounter complex. The adequacy

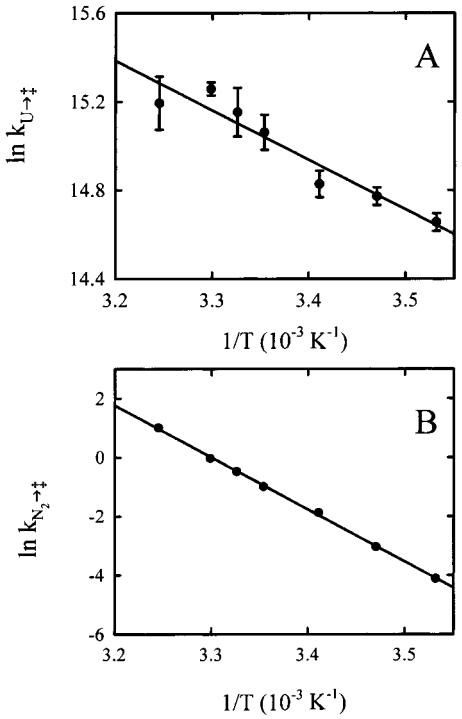

FIGURE 6: Arrhenius plot for the refolding (A) and unfolding (B) reactions. The values of $k_{U\rightarrow\ddagger}$ and $k_{N_2\rightarrow\ddagger}$ at each temperature were taken from the extrapolation to 0 M urea in the corresponding chevron plot. Lines represent first-order regressions [according to eq 17] to the data. Error bars are as shown or smaller than symbol size.

of diffusional models in describing protein folding has been pointed out extensively (*71*−*74*), and there are a number of examples in the literature supporting the fact that protein folding transitions can be explained as diffusional barrier-crossing processes (*75*−*79*), including GCN4-p2′ (*29*). In Kramers' theory, the measured rate constant is proposed to depend on the height of the activation barrier and the diffusion of reactants in the activated state. A value of 3.3×10^9 M^{-1} s^{-1} has been previously used for k_a for the diffusion-limited association reaction of a homodimeric coiled coil (*80*) and other dimeric systems (*10*). A value of 5×10^8 s^{-1} was used for k_a in the case of the unimolecular unfolding reaction (*10*), which is in the range observed for folding and intrachain diffusional collisions in small peptides (*81*−*85*).

Table 4: Thermodynamic Parameters Describing the Transition State for the Folding and Unfolding Reactions of M2V GCN4-p1 at 25 °C, According to the Kramers and Eyring Formalisms[a]

	$\Delta H^{\circ}_{i\rightarrow\ddagger}$[b] [kcal (mol of dimer)$^{-1}$]	$\Delta S^{\circ}_{i\rightarrow\ddagger}$ [cal (mol of dimer)$^{-1}$ K^{-1}]	$\Delta G^{\circ}_{i\rightarrow\ddagger}$ [kcal (mol of dimer)$^{-1}$]
2U → ‡			
Kramers	-1.6 ± 0.9	-19.04 ± 0.2[c]	4.1 ± 1.4[c]
Eyring	2.2 ± 0.9	-20.5 ± 2.8[c]	8.3 ± 1.7[c]
N_2 → ‡			
Kramers	30.8 ± 3.9	61.56 ± 13.3[d]	12.4 ± 5.0[d]
Eyring	34.6 ± 3.9	55.5 ± 13.3[d]	18.0 ± 5.0[d]

[a] Errors correspond to 2 standard deviations. [b] Eyring: values obtained from the slopes of the Arrhenius plots (Figure 6) according to eq 17. Kramers: values obtained from the slopes of the Arrhenius plots after correction by the temperature dependence of the water viscosity (*87*). [c] $\Delta G^{\circ}_{i\rightarrow\ddagger}$ and $\Delta S^{\circ}_{i\rightarrow\ddagger}$ values are dependent on the formalism employed to relate the rate constant to the activation energy (eq 18). They were calculated using $k_a = 3.3 \times 10^9$ M^{-1} s^{-1} and $k_a = k_B T/h = 6.2 \times 10^{12}$ s^{-1} for the Kramers and Eyring formalisms, respectively. [d] $\Delta G^{\circ}_{i\rightarrow\ddagger}$ and $\Delta S^{\circ}_{i\rightarrow\ddagger}$ were determined using $k_a = 5 \times 10^8$ and 6.2×10^{12} s^{-1} for the Kramers and Eyring formalisms, respectively.

According to transition-state theory, the activation enthalpies at 25 °C can be calculated, considering that $E_a = \Delta H_{i\rightarrow\ddagger} + RT$ (*86*): $\Delta H^{\circ}_{U\rightarrow\ddagger} = 2.2 \pm 0.9$ kcal (mol of dimer)$^{-1}$ and $\Delta H^{\circ}_{N_2\rightarrow\ddagger}$ 34.6 ± 3.9 kcal (mol of dimer)$^{-1}$. In Kramers' theory, the activation energy (derived from an Arrhenius plot) contains both the *true* activation enthalpy and the activation enthalpy reflecting the temperature dependence of the water viscosity [$\Delta H^{\circ}_{\ddagger,vis} = R\,\partial \ln \eta_0/\partial(1/T) = 3.8$ kcal mol^{-1} (*87*)]. Correcting for $\Delta H^{\circ}_{\ddagger,vis}$ yields the refolding and unfolding activation enthalpies, $\Delta H^{\circ}_{U\rightarrow\ddagger} = -1.6 \pm 0.9$ kcal (mol of dimer)$^{-1}$ and $\Delta H^{\circ}_{N_2\rightarrow\ddagger}$ 30.8 ± 3.9 kcal (mol of dimer)$^{-1}$, respectively.

Estimates for $\Delta S^{\circ}_{i\rightarrow\ddagger}$ and $\Delta G^{\circ}_{i\rightarrow\ddagger}$, at 25 °C in the absence of urea for the unfolding and refolding of M2V GCN4-p1, using both the Eyring and Kramers formalisms, are given in Table 4. According to the Kramers formalism, the energetic barrier for refolding is dominated by the activation entropy, whereas the unfolding barrier is dominated by the activation enthalpy. The small negative enthalpic component diminishes the refolding barrier; for the unfolding reaction, the activation barrier is diminished by the increase in entropy. This view is qualitatively in agreement with results obtained with the Eyring formalism.

DISCUSSION

Validity of the Two-State Assumption. Insights into the thermodynamic properties of the native, unfolded, and transition states of the coiled-coil M2V GCN4-p1 have been obtained by combining thermal- and urea-denaturation studies of both the equilibrium and kinetic folding reaction. Several lines of evidence support the two-state behavior of this dimeric peptide:

(a) The DSC experiments, performed at a variety of peptide concentrations (105−422 μM), yield a unitary ratio of $\Delta H^{\circ}_{cal}/\Delta H^{\circ}_{vH}$, within experimental error (Table 1). This observation has traditionally been considered as proof of a close adherence to a two-state equilibrium model (*60*, *88*), although recent arguments suggest that a unitary ratio may be a necessary but not sufficient condition (*89*).

(b) The observation of monophasic kinetics in both refolding and unfolding experiments (Figure 4) demonstrates that intermediate states are not significantly populated under these experimental conditions. The absence of a detectable burst phase and roll-over in the urea dependence of the rate constants obtained from individual fits are also consistent with the two-state kinetic mechanism.

(c) The good agreement between the enthalpy and entropy changes obtained from equilibrium (DSC experiments and the CD thermal melts) and kinetic studies (Table 2) supports the two-state model. Further support is provided by the excellent agreement between the *m* and ΔG° values obtained from kinetic experiments and from CD equilibrium measurements at different temperatures (Table 3).

The validity of the two-state assumption for M2V GCN4-p1 is also consistent with previous theoretical (*90*) and experimental reports of calorimetric (*20*, *21*, *23*) and spectroscopic (*22*, *24*, *91*) studies on the wild-type peptide and closely related analogues.

The use of two different perturbants, temperature and urea, to induce the unfolding reaction allows a comparison of the effects of these agents on the unfolded ensemble. To minimize errors associated with long extrapolations, 60 °C was selected as a reference temperature to compare the thermodynamic parameters obtained by DSC and the global analysis of the CD urea titrations and thermal melting profiles in the presence of urea: $\Delta H^{\circ}_{DSC} = 52.8$ kcal (mol of dimer)$^{-1}$, $\Delta S^{\circ}_{DSC} = 141$ cal (mol of dimer)$^{-1}$ K^{-1}, $\Delta G^{\circ}_{DSC} = 5.8$ kcal (mol of dimer)$^{-1}$, $\Delta H^{\circ}_{CD} = 49.6$ kcal (mol of dimer)$^{-1}$, $\Delta S^{\circ}_{CD} = 132$ cal (mol of dimer)$^{-1}$ K^{-1}, and $\Delta G^{\circ}_{CD} = 5.6$ kcal (mol of dimer)$^{-1}$. The excellent agreement among these values suggests that thermally induced and urea-induced unfolded states belong to the same thermodynamic ensemble. The observation of different far-UV ellipticities for the urea- and temperature-induced unfolded states (inset Figure 3; *92*−*95*) is consistent with the general view that chemical denaturation is more effective than thermal denaturation and, therefore, that the residual structure is less likely to exist in chemically denatured proteins (*96*). In fact, the predicted values for ΔC_p and *m* based on their empirical linear relationships with ΔASA_{pol} and ΔASA_{apol} for totally unfolded states (*97*), 680 cal (mol of dimer)$^{-1}$ K^{-1} and 0.91 kcal M^{-1} (mol of dimer)$^{-1}$, are in good agreement with the experimental values obtained from the global analysis of the urea-titration and thermal-denaturation experiments in the presence of urea, 556 cal (mol of dimer)$^{-1}$ K^{-1} and 0.82 kcal M^{-1} (mol of dimer)$^{-1}$, respectively. Furthermore, the existence of a certain degree of residual structure in the thermally unfolded chain has been experimentally shown by Holtzer and co-workers (*26*). By examining ^{13}C chemical shifts at specific sites of GCN4-lzK, a GCN4-like leucine zipper peptide, the authors concluded that the urea-unfolded

chain is randomly coiled, whereas the thermally unfolded chain retains a certain degree of structure.

Other findings support the presence of a relatively complex array of helical forms in the native state. Holtzer and colleagues have provided evidence for the existence of a native-state manifold and demonstrated site-specific differences in structural content and melting temperatures for GCN4-lzK, detected by ^{13}C NMR (*26*−*28*). Additionally, a stable folding subdomain of GCN4-p1, comprised of residues 8−30, has been proposed (*98*). The apparent discrepancy with the two-state analysis carried out in the present work probably arises from the global nature of the far-UV CD signal and from the existence of a single dominant barrier that separates two ensembles, each with many rapidly interconverting forms. Mohanty et al. (*90*) suggest that a *more relaxed* definition of the two-state model is necessary to account for the gradual conformational changes experienced by the *native*- and *unfolded*-state ensembles in the respective baseline regions.

Equilibrium Properties of M2V GCN4-p1. The stability of GCN4-p1 on a per-residue basis at 25 °C and standard state conditions [0.15 kcal (mol of res)$^{-1}$] is greater than that reported for a number of dimeric systems, such as Trp repressor [0.11 kcal (mol of res)$^{-1}$] and its fragment [2-66]$_2$ [0.11 kcal (mol of res)$^{-1}$] (*99*); Arc repressor [0.10 kcal (mol of res)$^{-1}$] (*100*); and SIV protease [0.07 kcal (mol of res)$^{-1}$] (*101*). This high degree of stability for the leucine zipper peptide is proposed to be the result of a densely packed hydrophobic interface comprised of branched aliphatic side chains (mainly Leu and Val). The important role of subunit interfaces in the stability of oligomeric proteins has been pointed out previously (*1*, *102*−*104*). Interestingly, a comparison with dimeric proteins of similar stability such as the four-α-helical-bundle protein ROP [0.15 kcal (mol of res)$^{-1}$] (*105*) and the N-terminal domain of LFB1, B1-Dim [0.18 kcal (mol of res)$^{-1}$] (*106*), yields a value for the change in enthalpy of unfolding for GCN4-p1 that is much higher [0.58 vs 0.23 and 0.32 kcal (mol of res)$^{-1}$ for ROP and B1-Dim, respectively]. This higher enthalpic contribution to stability for GCN4-p1 may reflect the very high helical content in the form of a single unbroken helix.

A calorimetric ΔC_p value of 406 ± 89 cal (mol of dimer)$^{-1}$ K^{-1} was measured for the unfolding of M2V GCN4-p1, in good agreement with previous results on the wild-type peptide (*21*, *23*) and a fragment containing the leucine zipper and a part of the basic region of GCN4 (*20*). The small discrepancies observed when comparing the enthalpy and entropy changes at 70 °C for the M2V mutant and the wild-type peptide [56.5 kcal (mol of dimer)$^{-1}$ and 152 cal (mol of dimer)$^{-1}$ K^{-1} vs 47.9 kcal (mol of dimer)$^{-1}$ and 128 cal (mol of dimer)$^{-1}$ K^{-1}, respectively] may reflect the presence of the formal charges at the termini in the wild-type peptide and the replacement of methionine by valine.

Structural Implications of the Temperature Dependence of $m_{N_2\rightarrow\ddagger}$ on the Native-State Ensemble. It has been shown previously that the *m* values extracted from equilibrium unfolding experiments correlate with the total buried surface area (*97*). Therefore, insights into the gross structural properties of the transition state can be obtained by examining the $m_{N_2\rightarrow\ddagger}$ and $m_{U\rightarrow\ddagger}$ values extracted from the analysis of the chevron plots at different temperatures and the *m* values from the equilibrium profiles (Table 3). Under the assumption that the ratio $m_{U\rightarrow\ddagger}/m$ is a measure of the position of the transition state along the unfolding reaction coordinate (*107*), the majority of the total change in surface area expected on going from the unfolded to the native state is buried in the dimeric transition state (between 55 and 65%, depending on the temperature). Previous studies have reported values of ∼55% for unmodified GCN4-p1 between 5 and 15 °C (*22*, *35*, *63*), in agreement with the present study.

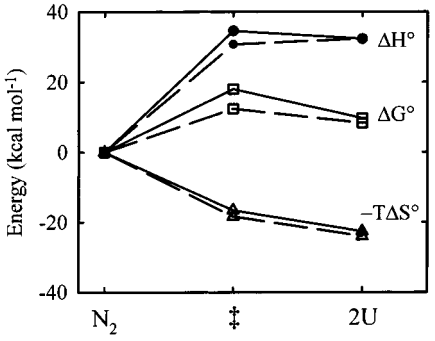

FIGURE 7: Reaction coordinate for M2V GCN4-p1 at a standard state of 25 °C and 0 M urea. N_2 was taken as a reference state, and its properties were arbitrarily set to zero. The values for $\Delta G^\circ_{i\rightarrow\ddagger}$, $\Delta H^\circ_{i\rightarrow\ddagger}$, and $\Delta S^\circ_{i\rightarrow\ddagger}$ were taken from Table 4. The reaction profiles were calculated using both the Kramers formalism, with preexponential factors of 3.3×10^9 M^{-1} s^{-1} and 5×10^8 s^{-1} (dashed lines), and the Eyring formalism, with a preexponential factor of $k_BT/h = 6.2 \times 10^{12}$ s^{-1} (solid lines).

Closer examination of the results in Table 3 shows that the decrease in m_{kn} with increasing temperature is almost entirely due to a monotonic decrease in $m_{N_2\rightarrow\ddagger}$, given that $m_{kn} = m_{N_2\rightarrow\ddagger} - m_{U\rightarrow\ddagger}$. This implies that fraying or local unfolding in the native ensemble is decreasing the amount of buried surface; the change in buried surface area between the unfolded ensemble and the transition state is not affected by temperature. This interpretation is consistent with the increasing ellipticity observed for the native baseline (Figure 2A) and previous NMR results that detect significant end-fraying of a GCN4-like peptide before the cooperative transition (*26*). Taken together, these results imply that the temperature dependence observed for $m_{N_2\rightarrow\ddagger}$ is a manifestation of a native-state ensemble of rapidly interconverting coiled-coil forms with decreasing amounts of helical structure at increasing temperature.

Energetics of the Transition-State Ensemble. On the basis of the kinetic data reported in this paper, a reaction coordinate diagram for M2V GCN4-p1 can be constructed (Figure 7). The data are shown at 25 °C, and the free energy, enthalpy, and entropy of the native form have been set to zero as a reference state. Values for $\Delta H^\circ_{i\rightarrow\ddagger}$, $\Delta G^\circ_{i\rightarrow\ddagger}$, and $\Delta S^\circ_{i\rightarrow\ddagger}$, according to the Eyring (solid lines in Figure 7) and Kramers (dashed lines in Figure 7) formalisms, are also provided. By either formalism, there is an increase in the entropy (decrease in $-T\Delta S^\circ$) when going from N_2 to U. Because the transition state is dimeric, the entropy change for $N_2 \rightarrow \ddagger$ only reflects partial unfolding of the coiled coil, whereas the value obtained for $\ddagger \rightarrow$ 2U reflects further unfolding and dissociation of the two chains. Because the majority of the entropy change occurs between N_2 and ‡, the translational/rotational entropy gain is not the dominant factor for the dissociation reaction. This conclusion is in accord with an estimate of 5 ± 8 cal mol^{-1} K^{-1} for the translational/rotational entropy

by Privalov and colleagues (*108*), on the basis of calorimetric measurements on a homodimeric coiled coil and its cross-linked version (*108*) and with other experimental (*109*−*111*) and theoretical (*112*) results. As has been pointed out by Karplus and Janin (*113*), this experimental value relates to the entropy for the dissociation of the native dimer to two unfolded polypeptide chains, whereas theoretical estimates of 30−60 cal mol^{-1} K^{-1} have been reported for the unfolding of a native dimer to two native monomers (*114*, *115*). It is not possible to ascertain the validity of either estimate for the translational/rotational entropy on the basis of the experimental value for the activation entropy observed for the association reaction of GCN4-p1. The large positive entropy of dehydration accompanying the formation of the transition state and the large negative contributions from helix formation and side-chain packing in the dimer interface make it impossible to accurately estimate the translational/rotational component.

The barrier for the unfolding reaction of M2V GCN4-p1 is dominated by enthalpic contributions (Figure 7), presumably arising from the disruption of H bonds and van der Waals interactions. The height of the activation barrier for the unfolding reaction is significantly diminished by an overall entropy gain because of the disruption of part of the helical structure (an increase in the backbone conformational entropy is expected to be on the order of 6 cal (mol of res)$^{-1}$ K^{-1} (*23*)) and the side-chain packing at the interface. By contrast, the barrier in the bimolecular folding is almost entirely accounted for by the activation entropy. This observation is not readily generalized to other dimeric systems because enthalpic barriers have been reported for the P-22 Arc repressor (*12*) and the Trp repressor (*10*).

General View of the Transition State of GCN4-p1. A critical aspect in defining the energy landscape of a folding reaction involves the characterization of the rate-limiting transition state(s). Mutational analysis (*35*) has shown that the transition state for GCN4-p1 involves the docking of helical stretches located primarily, although not exclusively, at the C termini of a pair of monomers. On the basis of these results, the following folding model for GCN4-p1 has been proposed:

$$U \overset{\text{very fast}}{\rightleftharpoons} I$$

$$I + I \overset{\text{rate-limiting step}}{\rightleftharpoons} N_2$$

A rapid equilibrium is established between the unfolded monomers and the monomeric intermediate I, which contains helical structure localized primarily in the C terminus. Under folding conditions, the concentration of the association-competent form I remains sufficiently low that the apparent rate constant observed for the association reaction is on the order of 10^6 M^{-1} s^{-1}. This value is approximately 3 orders of magnitude smaller than that of the diffusion limit, implying that not all collisions between monomers lead to the native dimer. According to this simple model, only collisions between association-competent species I are successful. Note that I is not a single structural form but rather an ensemble of rapidly interconverting species. Once the transition state is formed, the complex between preformed helical segments acts as a nucleation site to extend the helices toward the less-structured N terminus. This scenario for the folding reaction is consistent with both diffusion−collision and nucleation−condensation models (*116*).

The activation parameters extracted from the transition-state analysis carried out in the present study agree qualitatively with the above scenario. Perhaps the most informative result is the small nearly zero value for the refolding activation enthalpy change [−1.6 or 2.2 kcal (mol of dimer)$^{-1}$, depending on the formalism]. The observation that the transition state appears to bury about 55−65% of the urea-sensitive surface area combined with the results from previous studies in trifluoroethanol (*117*) suggests that the peptide chains undergo considerable desolvation upon folding. Thermodynamic data for the transfer of aliphatic nonpolar hydrocarbons from the pure liquid phase to water yield enthalpies of hydration in the range of 0 to −0.478 kcal mol^{-1} at room temperature (*46*, *118*). Therefore, if dehydration was the only event involved in surmounting the folding barrier, a large positive value for $\Delta H^{\circ}_{U\rightarrow\ddagger}$ should have been observed. The implied negative contribution from another source reflects the formation of intramolecular hydrogen bonds in the activated complex. This conclusion is consistent with the results of a study by Sosnick and coworkers, who explored the formation of H bonds during the folding reaction of GCN4 D7A using equilibrium and kinetic deuterium/hydrogen amide isotope techniques (*25*). These authors concluded that ∼50% of the native H bonds are formed in the transition state. On the basis of an estimated value of ∼ −0.84 kcal (mol of res)$^{-1}$ for the formation of a hydrogen bond in the coil−helix transition (*119*), the activation enthalpy should be decreased by ∼25 kcal mol^{-1} for the pair of helical segments in the dimeric transition state of M2V GCN4-p1. Therefore, the dehydration effect must almost exactly cancel the H-bond effect.

The activation entropy is also consistent with this model for the transition state. The entropic contribution to the barrier for the dimerization reaction is approximately −20 cal (mol of dimer)$^{-1}$ K^{-1} (Table 4). The burial of 55−65% of the urea-sensitive surface area in this step means that a substantial amount of dehydration must occur. On the basis of thermodynamic data of transfer of hydrocarbons from the liquid phase to water (*46*, *118*), the hydration entropy has been estimated to be negative at room temperature (reported values ranged from −13.8 to −26.0 cal mol^{-1} K^{-1}). Therefore, the negative entropy change observed in the refolding of M2V GCN4-p1 means that the contribution from dehydration is overwhelmed by the penalty of bringing two chains together and of ordering side chains and the backbone in the transition state.

Summary. Equilibrium and kinetic folding experiments on M2V GCN4-p1 have elucidated the features of its energy landscape. The unfolding barrier is mainly enthalpic, reflecting the disruption of a substantial fraction of the hydrogen bonds in the coiled-coil structure. The association reaction is primarily retarded by an entropic component, reflecting a delicate counterbalance between solvent effects and intramolecular interactions. These thermodynamic results are consistent with a previous proposal that the transition state is partially organized (*35*).

ACKNOWLEDGMENT

We thank Brandon Doyle for assistance with the ultracentrifugation experiments. We are also grateful to Drs.

Osman Bilsel, Ernesto Freire, Jonathan Goldberg, Roxana Ionescu, Marimar Lopez, Irene Luque, Jose Manuel Sanchez-Ruiz, and Jill Zitzewitz for valuable scientific discussions. We also thank Drs. Osman Bilsel, Roxana Ionescu, and Jill Zitzewitz for a critical reading of the manuscript.

REFERENCES

1. Jones, S., and Thornton, J. M. (1996) *Proc. Natl. Acad. Sci. U.S.A. 93*, 13−20.
2. Chen, B. L., Baase, W. A., and Schellman, J. A. (1989) *Biochemistry 28*, 691−699.
3. Chen, X., and Matthews, C. R. (1994) *Biochemistry 33*, 6356−6362.
4. Jackson, S. E., and Fersht, A. R. (1991) *Biochemistry 30*, 10436−10443.
5. Oliveberg, M., and Fersht, A. R. (1996) *Biochemistry 35*, 2738−2749.
6. Schindler, T., and Schmid, F. X. (1996) *Biochemistry 35*, 16833−16842.
7. Tan, Y. J., Oliveberg, M., and Fersht, A. R. (1996) *J. Mol. Biol. 264*, 377−389.
8. Parker, M. J., Lorch, M., Sessions, R. B., and Clarke, A. R. (1998) *Biochemistry 37*, 2538−2545.
9. Plaxco, K. W., Guijarro, J. I., Morton, C. J., Pitkeathly, M., Campbell, I. D., and Dobson, C. M. (1998) *Biochemistry 37*, 2529−2537.
10. Gloss, L. M., and Matthews, C. R. (1998) *Biochemistry 37*, 16000−16010.
11. Desai, G., Panick, G., Zein, M., Winter, R., and Royer, C. A. (1999) *J. Mol. Biol. 288*, 461−475.
12. Milla, M. E., and Sauer, R. T. (1994) *Biochemistry 33*, 1125−1133.
13. Lassalle, M. W., and Hinz, H. J. (1998) *Biochemistry 37*, 8465−8472.
14. Lassalle, M. W., and Hinz, H. J. (1999) *Biol. Chem. 380*, 459−472.
15. Wallace, L. A., Sluis-Cremer, N., and Dirr, H. W. (1998) *Biochemistry 37*, 5320−5328.
16. Crick, F. H. C. (1953) *Acta Crystallogr. 6*, 689−697.
17. Oas, T. G., McIntosh, L. P., O'Shea, E. K., Dahlquist, F. W., and Kim, P. S. (1990) *Biochemistry 29*, 2891−2894.
18. Goodman, E. M., and Kim, P. S. (1991) *Biochemistry 30*, 11615−11620.
19. O'Shea, E. K., Klemm, J. D., Kim, P. S., and Alber, T. (1991) *Science 254*, 539−544.
20. Thompson, K., Vinson, C., and Freire, E. (1993) *Biochemistry 32*, 5491−5496.
21. Kenar, K. T., Garcia-Moreno, B., and Freire, E. (1995) *Protein Sci. 4*, 1934−1938.
22. Zitzewitz, J. A., Bilsel, O., Luo, J., Jones, B. E., and Matthews, C. R. (1995) *Biochemistry 34*, 12812−12819.
23. D'Aquino, J. A., Gomez, J., Hilser, V. J., Lee, K. H., Amzel, L. M., and Freire, E. (1996) *Proteins*: *Struct., Funct., Genet. 25*, 143−156.
24. Durr, E., Jelesarov, I., and Bosshard, H. R. (1999) *Biochemistry 38*, 870−880.
25. Krantz, B. A., Moran, L. B., Kentsis, A., and Sosnick, T. R. (2000) *Nat. Struct. Biol. 7*, 62−70.
26. Holtzer, M. E., Lovett, E. G., d'Avignon, D. A., and Holtzer, A. (1997) *Biophys. J. 73*, 1031−1041.
27. d'Avignon, D. A., Bretthorst, G. L., Holtzer, M. E., and Holtzer, A. (1998) *Biophys. J. 74*, 3190−3197.
28. d'Avignon, D. A., Bretthorst, G. L., Holtzer, M. E., and Holtzer, A. (1999) *Biophys. J. 76*, 2752−2759.
29. Bhattacharyya, R. P., and Sosnick, T. R. (1999) *Biochemistry 38*, 2601−2609.
30. Moran, L. B., Schneider, J. P., Kentsis, A., Reddy, G. A., and Sosnick, T. R. (1999) *Proc. Natl. Acad. Sci. U.S.A. 96*, 10699−10704.
31. Jelesarov, I., Durr, E., Thomas, R. M., and Bosshard, H. R. (1998) *Biochemistry 37*, 7539−7550.
32. Wendt, H., Leder, L., Harma, H., Jelesarov, I., Baici, A., and Bosshard, H. R. (1997) *Biochemistry 36*, 204−213.
33. Wendt, H., Baici, A., and Bosshard, H. R. (1994) *J. Am. Chem. Soc. 116*, 6973−6974.
34. Wendt, H., Berger, C., Baici, A., Thomas, R. M., and Bosshard, H. R. (1995) *Biochemistry 34*, 4097−4107.
35. Zitzewitz, J. A., Ibarra-Molero, B., Fishel, D. R., Terry, K. L., and Matthews, C. R. (2000) *J. Mol. Biol. 296*, 1105−1116.
36. Edelhoch, H. (1967) *Biochemistry 6*, 1948−1954.
37. Pace, C. N., Shirley, B. A., and Thomson, J. A. (1989) in *Protein structure, a practical approach* (Creighton, T. E., Ed), pp 311−330, IRL Press at Oxford University Press, Oxford, U.K.
38. Makhatadze, G. I. (1998) *Curr. Protoc. Protein Sci. 2*, 7.9.1−7.9.14.
39. Plotnikov, V. V., Brandts, J. M., Lin, L. N., and Brandts, J. F. (1997) *Anal. Biochem. 250*, 237−244.
40. Mann, C. J., Shao, X., and Matthews, C. R. (1995) *Biochemistry 34*, 14573−14580.
41. Peterman, B. F. (1979) *Anal. Biochem. 93*, 442−444.
42. Makhatadze, G. I., Medvedkin, V. N., and Privalov, P. L. (1990) *Biopolymers 30*, 1001−1010.
43. Privalov, P. L., and Potekhin, S. A. (1986) *Methods Enzymol. 131*, 4−51.
44. Sturtevant, J. M. (1987) *Annu. Rev. Phys. Chem. 38*, 463−488.
45. Sanchez-Ruiz, J. M. (1995) *Subcell Biochem. 24*, 133−176.
46. Privalov, P. L., and Gill, S. J. (1988) *Adv. Protein Chem. 39*, 191−234.
47. Privalov, P. L. (1989) *Annu. Rev. Biophys. Biophys. Chem. 18*, 47−69.
48. Greene, R. F., and Pace, C. N. (1974) *J. Biol. Chem. 249*, 5388−5393.
49. Pace, N. C. (1986) *Methods Enzymol. 131*, 266−280.
50. Bernasconi, C. F. (1976) in *Relaxation kinetics*, Academic Press, New York.
51. Matthews, C. R. (1987) *Methods Enzymol. 154*, 498−511.
52. Chen, B. L., Baase, W. A., Nicholson, H., and Schellman, J. A. (1992) *Biochemistry 31*, 1464−1476.
53. Jacob, M., and Schmid, F. X. (1999) *Biochemistry 38*, 13773−13779.
54. Kawahara, K., and Tanford, C. (1966) *J. Biol. Chem. 241*, 3228−3232.
55. Ghosh, J. C., and Gyani, B. P. (1953) *J. Indian Chem. Soc. 30*, 350−354.
56. Woody, R. W. (1985) *Peptides (NY, 1979−1987) 7*, 15−114.
57. Swint, L., and Robertson, A. D. (1993) *Protein Sci. 2*, 2037−2049.
58. Kuhlman, B., and Raleigh, D. P. (1998) *Protein Sci. 7*, 2405−2412.
59. Freire, E. (1989) *Comments Mol. Cell. Biophys. 6*, 123−140.
60. Privalov, P. L. (1979) *Adv. Protein Chem. 33*, 167−241.
61. O'Shea, E. K., Rutkowski, R., and Kim, P. S. (1989) *Science 243*, 538−542.
62. Marky, L. A., and Breslauer, K. J. (1987) *Biopolymers 26*, 1601−1620.
63. Sosnick, T. R., Jackson, S., Wilk, R. R., Englander, W., and DeGrado, W. F. (1996) *Proteins 24*, 427−432.
64. Baldwin, R. L. (1996) *Folding Des. 1*, R1−8.
65. Kuwajima, K., Kim, P. S., and Baldwin, R. L. (1983) *Biopolymers 22*, 59−67.
66. Segawa, S. I., and Sugihara, M. (1984) *Biopolymers 23*, 2473−2488.
67. Scalley, M. L., and Baker, D. (1997) *Proc. Natl. Acad. Sci. U.S.A. 30*, 10636−10640.
68. Glasstone, S., Laidler, K. J., and Eyring, H. (1940) *Theory of Rate Processes*, McGraw-Hill, New York.
69. Beasty, A. M., and Matthews, C. R. (1985) *Biochemistry 24*, 3547−3553.
70. Kramers, H. A. (1940) *Physica 7*, 284−304.
71. Socci, N. D., Onuchi, J. N., and Wolynes, P. G. (1996) *J. Chem. Phys. 104*, 5860−5868.
72. Thirumalai, D., and Woodson, S. A. (1996) *Acc. Chem. Res. 29*, 433−439.
73. Klimov, D. K., and Thirumalai, D. (1997) *Phys. Rev. Lett. 79*, 317−320.

74. Zwanzig, R. (1997) *Proc. Natl. Acad. Sci. U.S.A. 94*, 148−150.
75. Chrunyk, B. A., and Matthews, C. R. (1990) *Biochemistry 29*, 2149−2154.
76. Waldburger, C. D., Jonsson, T., and Sauer, R. T. (1996) *Proc. Natl. Acad. Sci. U.S.A. 93*, 2629−2634.
77. Jacob, M., Schindler, T., Balbach, J., and Schmid, F. (1997) *Proc. Natl. Acad. Sci. U.S.A. 94*, 5622−5627.
78. Jacob, M., Geeves, M., Holtermann, G., and Schmid, F. (1999) *Nat. Struct. Biol. 6*, 923−926.
79. Plaxco, K. W., and Baker, D. (1998) *Proc. Natl. Acad. Sci. U.S.A. 95*, 13591−13596.
80. Ozeki, S., Kao, T., Holtzer, M. E., and Holtzer, A. (1991) *Biopolymers 8*, 957−966.
81. Dill, K. A., and Chan, H. S. (1997) *Nat. Struct. Biol. 4*, 10−19.
82. Eaton, W. A., Munoz, V., Thompson, P. A., Chan, C. K., and Hofrichter, J. (1997) *Curr. Opin. Struct. Biol. 7*, 10−14.
83. Thompson, P. A., Eaton, W. A., and Hofrichter, J. (1997) *Biochemistry 36*, 9200−9210.
84. Munoz, V., Thompson, P. A., Hofrichter, J., and Eaton, W. A. (1997) *Nature 390*, 196−199.
85. Munoz, V., Henry, E. R., Hofrichter, J., and Eaton, W. A. (1998) *Proc. Natl. Acad. Sci. U.S.A. 95*, 5872−5879.
86. Atkins, P. W. (1986) *Physical Chemistry*, Freeman and Co., New York.
87. *Handbook of Chemistry and Physics* (Weast, R. C., Ed), 53rd ed., F36, Chemical Rubber Co., Cleveland, OH.
88. Schellman, J. A. (1987) *Annu. Rev. Biochem. 16*, 115−137.
89. Zhou, Y., Hall, C. K., and Karplus, M. (1999) *Protein Sci. 8*, 1064−1074.
90. Mohanty, D., Kolinski, A., and Skolnick, J. (1999) *Biophys. J. 77*, 54−69.
91. Jelesarov, I., and Bosshard, H. R. (1996) *J. Mol. Biol. 263*, 344−358.
92. Pace, N. C., and Tanford, C. (1968) *Biochemistry 7*, 198−208.
93. Robertson, A. D., and Baldwin, R. L. (1991) *Biochemistry 30*, 9907−9914.
94. Agashe, V. R., and Udgaonkar, J. B. (1995) *Biochemistry 34*, 3286−3299.
95. Scholtz, J. M. (1995) *Protein Sci. 4*, 35−43.
96. Tanford, C. (1968) *Adv. Protein Chem. 23*, 121−275.
97. Myers, J. K., Pace, C. N., and Scholtz, J. M. (1995) *Protein Sci. 4*, 2138−2148.
98. Lumb, K. J., Carr, C. M., and Kim, P. S. (1994) *Biochemistry 33*, 7361−7367.
99. Gloss, L. M., and Matthews, C. R. (1997) *Biochemistry 36*, 5612−5623.
100. Bowie, J. U., and Sauer, R. T. (1989) *Biochemistry 28*, 7139−7143.
101. Grant, S. K., Deckman, I. C., Culp, J. S., Minnich, M. D., Brooks, I. S., Hensley, P., Debouck, C., and Meek, T. D. (1992) *Biochemistry 31*, 9491−9501.
102. Miller, S., Lesk, A. M., Janin, J., and Chothia, C. (1987) *Nature 27*, 834−836.
103. Larsen, T. A., Olson, A. J., and Goodsell, D. S. (1998) *Structure 6*, 421−427.
104. Xu, D., Tsai, C.-J., and Nussinov, R. (1998) *Protein Sci. 7*, 533−544.
105. Steif, C., Weber, P., and Hinz, H.-J. (1993) *Biochemistry 32*, 3867−3876.
106. De Francesco, R., Pastore, A., Vecchio, G., and Cortese, R. (1991) *Biochemistry 30*, 143−147.
107. Matouschek, A., and Fersht, A. R. (1993) *Proc. Natl. Acad. Sci. U.S.A. 90*, 7814−7818.
108. Yu, Y. B., Lavigne, P., Kay, C. M., Hodges, R. S., and Privalov, P. L. (1999) *J. Phys. Chem. 103*, 2270−2278.
109. Murphy, K. P., Xie, D., Thompson, K. S., Amzel, L. M., and Freire, E. (1994) *Proteins 18*, 63−67.
110. Gomez, J., and Freire, E. (1995) *J. Mol. Biol. 252*, 337−350.
111. Tamura, A., and Privalov, P. L. (1997) *J. Mol. Biol. 273*, 1048−1060.
112. Amzel, L. M. (1997) *Proteins*: *Struct., Funct., Genet. 28*, 144−149.
113. Karplus, M., and Janin, J. (1999) *Protein Eng. 12*, 185−186.
114. Finkelstein, A. V., and Janin, J. (1989) *Protein Eng. 3*, 1−3.
115. Tidor, B., and Karplus, M. (1993) *Proteins*: *Struct., Funct., Genet. 15*, 71−79.
116. Bilsel, O., and Matthews, C. R. (2000) *Adv. Protein Chem. 53*, 153−207.
117. Kentsis, A., and Sosnick, T. R. (1998) *Biochemistry 37*, 14613−14622.
118. Baldwin, R. L. (1986) *Proc. Natl. Acad. Sci. U.S.A. 83*, 8069−8072.
119. Richardson, J. M., McMahon, K. W., MacDonald, C. C., and Makhatadze, G. I. (1999) *Biochemistry 38*, 12869−12875.

BI001438E